ELSEVIER

Colloids and Surfaces B: Biointerfaces 19 (2000) 61–80

COLLOIDS AND SURFACES B

www.elsevier.nl/locate/colsurfb

Erythrocyte attachment to substrates: determination of membrane tension and adhesion energy

K.D. Tachev [a], J.K. Angarska [b], K.D. Danov [c], P.A. Kralchevsky [c,*]

[a] *Faculty of Biology, University of Shoumen, Shoumen 9712, Bulgaria*
[b] *Faculty of Chemistry, University of Shoumen, Shoumen 9712, Bulgaria*
[c] *Laboratory of Thermodynamics and Physicochemical Hydrodynamics, Faculty of Chemistry, University of Sofia, Sofia 1126, Bulgaria*

Received 15 November 1999; accepted 29 November 1999

Abstract

The adhesion of osmotically swollen erythrocytes to glass substrates is studied. An experimental set up is used, which allows one to carry out measurements with the same adherent cell at various compositions of the medium. The reflection interference microscopy is combined with the generalized Laplace equation describing the shape of the cell membrane. The latter equation, which accounts for the membrane bending elasticity, is solved numerically along with appropriate boundary conditions; the necessary values of some geometrical parameters are extracted from the interference data. The mathematical problem has a unique solution, which gives the values of the membrane tension, the pressure drop across the membrane, and the energy of adhesion. To reveal the physical origin of the observed cell-to-glass adhesion we carried out experiments with untreated (native) erythrocytes, as well as with trypsin-treated and glycophorin-treated erythrocytes. The former and the latter treatment, respectively, decreases and increases the outer surface electric charge of the cell. The comparison of the determined adhesion energies for untreated and trypsin-treated erythrocytes indicates that the adhesion could be attributed to the short-range electrostatic attraction due to the discreteness of the surface charge. The results for the glycophorin-treated erythrocytes show that at 20°C there is no cell-to-glass adhesion at all, whereas at 37°C adhesion is observed, but it is weaker than for untreated cells; this could be explained with the enhancement of the electrostatic double layer repulsion by the incorporation of additional electrically charged glycophorin molecules in the cell membrane. The developed mathematical and numerical procedure for solving the generalized Laplace equation can find application for interpreting the configurations of biological and model membranes (vesicles), both free and attached, and can bring information about physical parameters, such as membrane tension, difference in pressure or electric potential across the membrane, its bending elasticity and spontaneous curvature, energy of adhesion, etc.

Keywords: Adhesion of red blood cells; Bending elasticity; Erythrocyte osmotic swelling; Glycophorin incorporation; Membrane tension; Shape of cells; Trypsin treatment

* Corresponding author. Tel.: +359-2-9625310; fax: +359-2-9625643.
E-mail address: pk@ltph.bol.bg (P.A. Kralchevsky).

0927-7765/00/$ - see front matter
PII: S0927-7765(99)00164-2

1. Introduction

The circulation of the blood in vessels is accompanied with cell–cell and cell–wall collisions, which could lead to adhesion. The blood cell adhesion is influenced by various surface forces: electrostatic, hydration, steric, van der Waals and specific chemical bonding [1]; a number of theoretical models has been developed [2–4]. Their applicability depends on the stage of adhesion [2,5], the shape of the cell and the properties of the cell membrane (including glycocalyx) [3,6], the nature of the substrate [7,8]. Precise experimental methods have been applied to study the cell adhesion — reflection interference microscopy [5,8–11], double-view microscopy [12], electronic microscopy [13] and total internal reflection microscopy [14–16].

It has been established that the treatment of leaving erythrocytes with the enzyme trypsin (which decreases the surface charge of the cells) and the variation of the ionic strength of the medium influences the adhesion ability of erythrocytes [17,18]. To quantify the adhesion, the centrifugal force required for detachment of the trypsin treated cells from the glass substrate has been measured [17]. The results show that the increase of the ionic strength makes the detachment easier, but it is not clear whether the adhesive energy per unit area actually decreases, or the area of the adhesion film shrinks, or both of them take place.

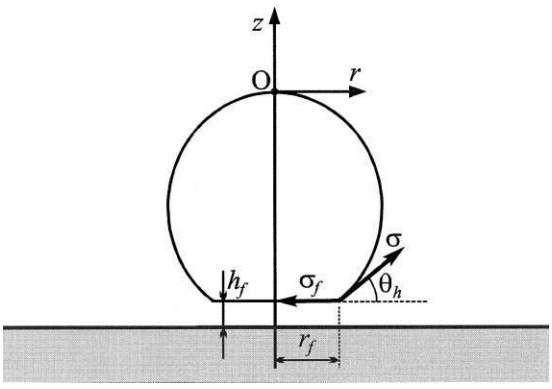

Fig. 1. Sketch of a swollen erythrocyte attached to a glass substrate; h_f is the thickness of the adhesion film, r_f is its radius, θ_h is contact angle, σ_f and σ are the tensions of the adherent and non-adherent portions of the cell membrane.

The colloid chemistry provides an alternative approach to determine the adhesion energy. As shown by Derjaguin [19] and Princen and Mason [20], the contact angle at the periphery of a liquid film is determined by the interaction between its surfaces. Hence, the adhesion energy can be determined by measuring the contact angle, say with the help of the reflection interference microscopy. As an illustration, Fig. 1 shows schematically the adhesion film between a cell and a substrate. The membrane tension of the cell in the zone of the adhesive film, σ_f, is somewhat smaller than the membrane tension of the free cell membrane, σ, because of the interaction across the adhesion film [21]:

$$\sigma_f = \sigma - w_a \quad (1)$$

Here w_a is the work (energy) of adhesion per unit area of the film. Force balance considerations (Fig. 1) yield a counterpart of the Young equation for a thin film [21]:

$$\sigma_f = \sigma \cos \theta_h \quad (2)$$

where θ_h is the contact angle of the film with thickness h. Combining Eqs. (1) and (2) one obtains

$$w_a = \sigma(1 - \cos \theta_h) \quad (3)$$

which is a form of the Dupré equation. Eq. (3) allows one to calculate the adhesion energy, w_a, if the values of the membrane tension, σ, and the contact angle, θ_h, are known.

In a previous study [5] we applied an interferometric method to study the adhesion of live osmotically swollen erythrocytes to glass substrates. It was established that the variation of the total solution osmolarity at constant ionic strength did not affect the film thickness, but did change the contact angle. Two major difficulties were encountered in [5]: (i) because of the differences between the individual studied erythrocytes (in size, age, membrane tension, etc.), it was not possible to distinguish whether the observed variation of θ_h is really due to the variation of solution osmolarity, or it is essentially affected by the individual properties of the various cells used in

the separate adhesion experiments, and (ii) the interferometric method gave the values of $\theta_{//}$, but the membrane tension σ, which increases with the swelling of the erythrocyte, was not known; for that reason w_a was not calculated.

In the present work we overcome these two difficulties in the following way: (i) we carry out experiments at a single cell level in an experimental chamber, which enables one to make measurements with the same cell at different osmolarities of the solution, and (ii) a theoretical model is applied, which allows to determine the membrane tension σ from the interference data for various osmolarities. Thus we can quantify w_a and the pressure difference ΔP across the cell membrane.

The experimental technique, combined with the theoretical model, is applied to investigate the adhesion to glass substrates of (a) native erythrocytes, (b) erythrocytes treated with the enzyme trypsin, and (c) erythrocytes treated with glycophorin.

The paper is structured as follows: Section 2 describes the preparation of the erythrocyte suspensions, the used experimental chamber, the microscopic and interferometric measurements; Section 3 outlines the procedures of data processing by solving the generalized Laplace equation and determining the membrane tension and adhesion energy; Section 4 presents numerical results and discussion; Appendix A gives details about the used solutions; Appendix B describes the procedures for treatment of erythrocytes with glycophorin; and finally, Appendix C presents the mathematical and numerical procedures for solving the generalized Laplace equation.

2. Experiments on erythrocyte adhesion

2.1. Preparation of the erythrocyte suspensions

The composition of the solutions applied in our experiments (such as the isotonic and hypotonic Tris-buffer, trypsin solution, etc.) are described in Appendix A. Human erythrocytes from blood groups 'A' and 'O', factor Rh(+), were used. They were isolated from venous blood samples stabilized with heparin (product of Spofa, Prague) by centrifugation at $1000 \times g$ for 20 min and triple washing with isotonic Tris-buffer solution, applying a procedure described in [5]. After the last centrifugation the buffer was removed by aspiration and the erythrocytes remained at the bottom of the test tube. Next, to prepare a stock suspension, isotonic Tris-buffer solution was added in such amount that the erythrocyte volume fraction was $\approx 50\%$. The stock suspension thus obtained was stored at 4°C and used within 2–3 days.

In our interferometric experiments (see below) we investigated erythrocytes whose shape is close to spherical. Such shape was achieved by re-suspending the erythrocytes in hypotonic Tris-buffer solution with osmolarity higher than the critical one (that corresponding to cell lysis). At osmolarity lower than the physiological one the osmotic effect causes an increase in the erythrocyte volume at almost constant area of the cell membrane. This corresponds to a transformation of the erythrocyte shape from biconcave disk to sphere. Further decrease of the osmolarity leads to an additional swelling of the cell and to increase of the membrane area and tension.

It is worthwhile noting that two regimes of membrane expansion have been identified [22,23]: (i) for small values of the relative dilatation, α, ($\alpha \equiv \Delta A/A$, A is the membrane area, ΔA is the increment of A) an apparent stretching of the membrane takes place, which consists in a flattening of thermally-excited undulations; in this regime $\ln \sigma \propto \alpha$, and (ii) for larger values of α a direct elastic stretch of the molecular surface area happens; in this regime $\sigma \propto \alpha$. The erythrocyte membrane cannot resist a direct elastic stretch > 2–4% [24].

At osmolarity of 131 mOsm, determined as a critical one, a cell lysis occurs [25]. In fact, the occurrence of lysis depends on the cell age, the individual properties of the membrane, the temperature and the electrolyte concentration. For the erythrocytes used in the present study at concentration of NaCl 4.5×10^{-2} M, at temperature 20°C, it has been found that the critical osmolarity is 135 mOsm. We investigated erythrocytes of various extent of swelling, which is obtained by varying the osmolarity of the medium (hypotonic

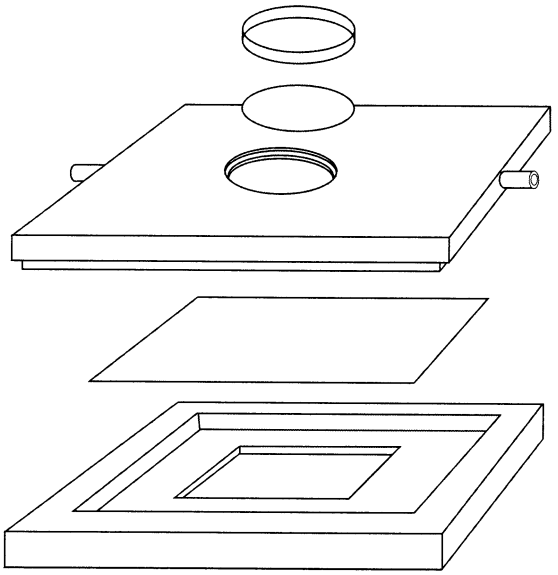

Fig. 2. Drawing of the used horizontal rectangular chamber of volume 0.72 cm^3 for investigation of cell adhesion. The lower part is a frame with a 24×60 mm cover glass to which the erythrocytes adhere; the upper part has a circular cover glass with a diameter of 18 mm. The aqueous medium inside the chamber can be exchanged by injection of a new solution.

Tris-buffer solution $+ 4.5 \times 10^{-2}$ M NaCl) from 156 down to 143 mOsm by addition of sucrose. The degree of swelling (as well as the membrane area and tension) increases with the decrease of osmolarity.

2.2. The experimental chamber

Fig. 2 presents the rectangular horizontal chamber used by us, which is similar to the standard perfusion chambers. It consists of two parts. The lower one is a frame containing a cover glass (24×60 mm) to which the erythrocytes adhere. In the upper part of the chamber a circular cover glass with a diameter of 18 mm is mounted. Both cover glass plates are products of Fisher Scientific. Parafilm flame gaskets were used to tight the two parts of the chamber and the glass plates. This small chamber of volume 0.72 cm^3 enables one to easily exchange the medium around the cells attached to the glass substrate and to investigate at a single cell level how the erythrocyte adhesion depends on the properties of the surrounding medium.

In our experiments an erythrocyte suspension of a given osmolarity (from 143 up to 153 mOsm) were supplied to the experimental chamber by means of an infusion pump with a rate of 90 ml/h. Next, the chamber was kept quiescent for 2 h. During that period erythrocytes sedimented at the bottom of the chamber and some of them did adhere at the rectangular glass substrate. Further, the chamber was turned with the upper side down and was kept in this position for another couple of hours to allow the non-adhered erythrocytes to detach from the substrate. Then the suspension was gradually replaced by infusion of buffer solution at a rate of 20 ml/h.

In the experiments examining the effect of osmolarity the interior of the chamber with the adherent erythrocytes was exchanged with other hypotonic buffer solution. The erythrocytes in the chamber were adherent to the glass substrate, so one could vary the osmolarity by gently ejecting the previous medium and simultaneously injecting solution with another desired osmolarity. Finally, the chamber was restored in its initial position and was carefully placed in a thermostat jacket on the microscope stage.

2.3. Microscopic and interferometric measurements

The erythrocytes adhered to the glass plate were observed from below in reflected monochromatic light (wavelength $\tilde{\lambda} = 551$ nm). Metalographic microscope 'Epitip 2' (Carl Zeiss, Jena) was used. Under these conditions Newton interference rings appear in the zone of contact of the cell with the substrate (Fig. 3). The interference pattern brings information about the shape of the cell membrane, which is analyzed below. We recorded the interference pattern by means of a video camera (Kyocera K10-HI70, Japan). Separate video-frames were stored in a computer by a frame grabber (Micro-Computer Products AG) and then they were processed by means of an image-analysis program (Mocha 1.2, Jandel Scientific). Thus the radii of the Newton interference rings were determined.

Some cells showed interference fringes, which deviated from the circular shape. We processed

only the interference pattern of cells, which exhibit circular fringes. The diameters of the rings of maximum and minimum intensity have been determined in independent measurements along four different radial directions, and then the average value of each diameter was taken.

As an example, Fig. 3(A) shows a photograph of the interference patterns in the zone of contact between untreated (native) erythrocytes and the glass substrate. The medium is hypotonic Tris-buffer solution of osmolarity 151 mOsm. The dark circular spot in the middle is the area of the adhesive film. The image analysis allows us to distinguish whether there is, or is not, a real adhesive film (Fig. 1). The latter appears as a spot of, respectively, uniform or nonuniform darkness (brightness) at the center of the interference pattern. The cells in Fig. 3(A) have formed a real adhesive film. The film diameter, $2r_f = 1.6 \pm 0.2$ μm, is measured from the photograph for the cell pointed by an arrow.

Fig. 3(B) shows a photograph of the interference patterns from attached trypsin-treated erythrocytes (see Section 4.2 for details). The diameter of the adhesive film (the dark spot in the middle) of the arrow-pointed cell is $2r_f = 1.4 \pm 0.2$ μm.

Fig. 3(C) shows a photograph of the interference patterns from adherent glycophorin-treated erythrocytes (see Appendix B about their preparation). Note that in this case the scale is different from Fig. 3(A, B). The spot in the middle of the interference pattern of glycophorin-treated cells is bright in contrast to those in Fig. 3(A, B), which implies that the thickness of the adhesive film is greater. The measured diameter of the adhesive film for the cell pointed by an arrow is $2r_f = 1.0 \pm 0.2$ μm. The fact that the thickness is greater and r_f is smaller for the glycophorin-treated erythrocytes can be attributed to the larger electrostatic repulsion between the cell and the substrate, enhanced by the additionally incorporated charged glycophorin molecules. More experimental data are given in Section 4 below.

3. Data processing; determining the cell shape

3.1. Mean membrane curvature in the fringe zone

To obtain information about the erythrocyte shape from the interference pattern, we first determine the mean curvature of the membrane in the zone, in which the interference rings are observed. In fact, each curved surface can be locally approximated with a sphere. The radius, R, of this sphere characterizes the local mean curvature of the surface [26]. To determine R in the zone of the fringes, we apply a theoretical approach from our previous paper [5].

The interference rings of maximum intensity are loci of points, for which the thickness, H_k, of the gap between the cell membrane and the glass substrate (Fig. 4) satisfy the condition

$$H_k = k\frac{\tilde{\lambda}}{4n}, \qquad k = 1,2,3,\ldots \tag{4}$$

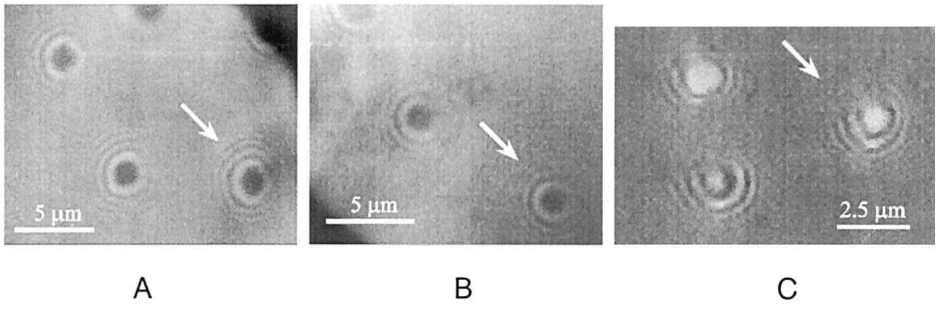

Fig. 3. Photographs of the interference pattern in the zone of contact between cells and a glass substrate. (A) Untreated erythrocytes; the medium is hypotonic solution of osmolarity 151 mOsm at 20°C. (B) Trypsin-treated erythrocytes at the same osmolarity and temperature. (C) Glycophorin-treated erythrocytes at osmolarity 153 mOsm at 37°C.

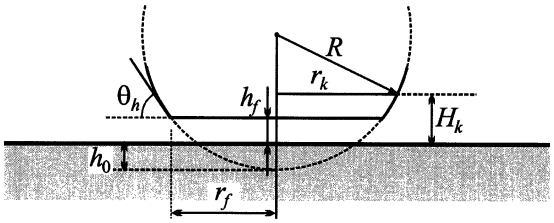

Fig. 4. Sketch of the zone of attachment of a swollen erythrocyte to a glass substrate; θ_h is the contact angle, H_k and r_k are running coordinates in the zone of the interference fringes; R is the local curvature radius in this zone; h_f and r_f denote the thickness and the radius of the adhesion film.

Here $\tilde{\lambda}$ is the wavelength of light, n is the refractive index of the aqueous medium, k is odd for the bright fringes and even for the dark ones. In fact H_k represents the local distance between the lipid bilayer of the cell membrane and the glass surface. In other words, in this treatment the outer glycocalyx of the erythrocyte belongs to the aqueous gap (film) between the cell and the glass surface. We fitted the data about the interference rings with the equation of a sphere with radius R. The radius r_k of the kth interference ring is assumed to obey the equation

$$(R - h_o - H_k)^2 + r_k^2 = R^2 \quad (5)$$

Here h_o is a geometrical parameter representing the distance between the apex of the extrapolated sphere and the glass surface (Fig. 4); R and h_o are to be determined from the best fit of the data (Fig. 5). Eq. (5) can be transformed to read

$$H_k^2 + r_k^2 = 2(R - h_o)H_k + (2R - h_o)h_o \quad (6)$$

As already mentioned, the values of H_k and r_k are obtained experimentally from the interference pattern. Then in view of Eq. (6) R and h_o can be determined from the slope and intercept of the plot of $H_k^2 + r_k^2$ versus H_k [5].

As an illustration, Fig. 5 shows plots of experimental data for $H_k^2 + r_k^2$ versus H_k obtained with a native erythrocyte for three different values of the osmolarity; the straight lines are the best fits drawn in accordance with Eq. (6). From the slope and the intercept one calculates $R = 3.9$, 3.4, 2.9 (± 0.15) μm and $h_o = 11.2$, 17.8, 47.8 nm, respectively, for osmolarities 143, 153 and 156 mOsm. Hence, it turns out that the local mean curvature radius, R, decreases with the rise of osmolarity. Moreover, the positive values of h_o confirm that there is really a flat adhesion film in the zone of contact (if h_o were negative, this would mean that the extrapolated membrane surface does not intersect the surface of the substrate, i.e. film is not formed; Fig. 4).

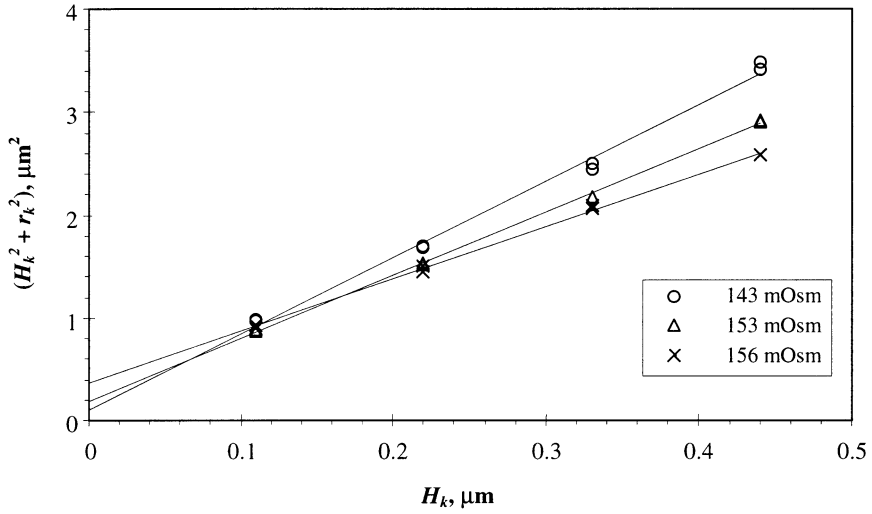

Fig. 5. Plots of $H_k^2 + r_k^2$ vs. H_k for the same native erythrocyte at three values of the solution osmolarity. The straight lines are drawn in accordance with Eq. (6).

In principle, knowing R, h_o, and the film radius r_f, from Eq. (5) one can estimate the film thickness h_f (Fig. 4). Unfortunately, a relatively small experimental error in the value of r_f leads to a large error in the calculated h_f. For that reason we do not use this approach to calculate h_f. On the other hand, the measured film radius r_f allows one to calculate the contact angle θ_h:

$$\sin \theta_h = \frac{r_f}{R} \tag{7}$$

The good agreement between the interferometric data and the straight lines drawn in accordance with Eq. (6) in Fig. 5 means that in the relatively narrow zone of the interference fringes the membrane shape can be locally approximated with a sphere. However, the shape of the erythrocyte as a whole can exhibit some deviation from sphere. The shape of the cell membrane is described by the generalized Laplace equation, which in this case (axisymmetric shape) is a fourth-order ordinary differential equation (Section 3.2). We will utilize the value of R, determined as explained above, in one of the boundary conditions necessary for solving this equation.

3.2. Differential equation describing the cell shape

To calculate the adhesion energy, $w_a = \sigma(1 - \cos \theta_h)$, see Eq. (3), we need to determine not only the contact angle, θ_h, but also the membrane tension, σ. As demonstrated below, the value of σ for a given state of a cell can be found with the help of the generalized Laplace equation.

The shape of biological and model membranes is usually determined by minimization of an appropriate expression for the free energy of the system [24,27–34]. For example, the elastic energy of tension-free membranes is given by the energy of bending [27]

$$W_B = \int [\tfrac{1}{2} k_c (c_1 + c_2 - c_0)^2 + \bar{k}_c c_1 c_2] \mathrm{d}A \tag{8}$$

In Eq. (8) the integration is carried out over the surface of the membrane; c_1 and c_2 are the two principal curvatures of the membrane which vary from point to point; c_0, k_c and $\bar{k}_c$ are constant parameters of the mechanical model termed, respectively, spontaneous curvature, bending and Gaussian curvature elasticity. Other mechanical models of erythrocyte membranes involve other parameters such as stretching and shearing elasticity [24,30].

A potentially powerful approach is based on a differential equation describing the shape of membranes, which represents a generalization of the Laplace equation of capillarity [35–39]. In general, it is a complicated partial differential equation, but for axisymmetric shapes (like our adherent cells) it reduces to a set of two ordinary differential equations [38]:

$$\sigma\left(\frac{\mathrm{d} \sin \theta}{\mathrm{d}r} + \frac{\sin \theta}{r}\right) + \eta\left(\frac{\mathrm{d} \sin \theta}{\mathrm{d}r} - \frac{\sin \theta}{r}\right) = \Delta P + \frac{k_c}{r} \cos \theta \frac{\mathrm{d}}{\mathrm{d}r}\left\{ r \cos \theta \frac{\mathrm{d}}{\mathrm{d}r}\left[\frac{1}{r} \frac{\mathrm{d}}{\mathrm{d}r}(r \sin \theta) \right] \right\} \tag{9}$$

$$\frac{\mathrm{d}z}{\mathrm{d}r} = \tan \theta \tag{10}$$

where θ is the running slope angle. Eqs. (9) and (10) determine the generatrix of the membrane profile in a parametric form: $r = r(\theta)$, $z = z(\theta)$, where r and z are the common cylindrical coordinates (Fig. 1). In the generalized Laplace equation, Eq. (9), η is the shearing tension and ΔP is the pressure difference across the membrane. For $\eta = 0$ and $k_c = 0$ Eq. (9) reduces to the common Laplace equation of capillarity, which describes the various shapes of fluid interfaces [40]. The approach based on Eq. (9) is equivalent to the approach based on the expression for the free energy, insofar as the generalized Laplace equation is derived by minimization of the free energy, see, e.g. [39].

The form of Eq. (9) calls for discussion. The expression for W_B, Eq. (8), which is involved in the derivation of Eq. (9), contains the parameters spontaneous curvature, c_0, and Gaussian elasticity, $\bar{k}_c$, while the latter two parameters are missing in Eq. (9). It has been rigorously proven that c_0 and $\bar{k}_c$ must not enter the generalized Laplace equation [38]; on the other hand, c_0 and $\bar{k}_c$ can enter the solution through the boundary conditions [39]. For example, Deuling and Helfrich [29] described the myelin forms of an erythrocyte

membrane assuming tension-free state of the membrane, that is $\sigma = \eta = 0$ and $\Delta P = 0$; then they calculated the shape of the membrane as a solution of the equation

$$\frac{1}{r}\frac{\mathrm{d}}{\mathrm{d}r}(r \sin\theta) = c_0 = \text{constant} \tag{11}$$

It is obvious that for $\sigma = \eta = 0$ and $\Delta P = 0$ every solution of Eq. (11) satisfies Eq. (9), and that c_0 appears as a constant of integration.

Coming back to the swollen adherent erythrocytes, we should note that in our case we must not set $\sigma = 0$ and $\Delta P = 0$, since the membrane is expected to have some tension, even a very low one. On the other hand, to simplify our treatment we will set $\eta = 0$ in Eq. (9), i.e. we will neglect the effect of the shearing tension. Setting $\eta = 0$ means that the stresses in the membrane are assumed to be tangentially isotropic, that is the membrane behaves as a two-dimensional fluid. In fact, there are some experimental indications that $\eta \ll \sigma$ [24,41]. Thus we will seek the membrane profile as a solution of the equation

$$\sigma\left(\frac{\mathrm{d}\sin\theta}{\mathrm{d}r} + \frac{\sin\theta}{r}\right) = \Delta P + \frac{k_c}{r}\cos\theta\frac{\mathrm{d}}{\mathrm{d}r}\left\{r\cos\theta\frac{\mathrm{d}}{\mathrm{d}r}\left[\frac{1}{r}\frac{\mathrm{d}}{\mathrm{d}r}(r\sin\theta)\right]\right\} \tag{12}$$

To find the solution of Eq. (12), along with Eq. (10), one needs four boundary conditions. Moreover, Eq. (12) contains two material parameters: k_c/σ and $\Delta P/\sigma$. The six unknown parameters (four integration constants + two material parameters) can be determined from the following six conditions: (i–ii) $z = 0$ and $\theta = 0$ at $r = 0$, i.e. at the apex of the membrane (the point where the membrane intersects the z-axis, point O in Fig. 1); (iii) the membrane curvature varies smoothly in a vicinity of the membrane apex; (iv) $\theta = \theta_h$ for $r = r_f$ (Fig. 1); (v) the total area of the membrane, A_T, is known (see Section 4 for details); and (vi) ΔP is determined from the experimental value of R (Section 3.1) and the common Laplace equation:

$$\Delta P = 2\sigma/R \tag{13}$$

The usage of Eq. (13) is justified because in the zone of the interference fringes the membrane profile can be approximated well by a sphere of radius R (see Fig. 5 and Section 3.1).

Alternatively, instead of using the condition (vi) and the procedure from Section 3.1, one can directly fit the interference data with Eq. (12). Such an approach leads to a numerical minimization procedure with three variable parameters (cf. Eq. (33) below), which are to be determined from the best fit. We preferred to obtain, in advance, (Section 3.1) the value of one of the three parameters (viz. R) and thus to facilitate the minimization procedure.

We integrated numerically Eq. (12), along with Eq. (10), determining the six unknown parameters from the conditions (i)–(vi). The mathematical and numerical procedure, which is not trivial, is described in detail in Appendix C. From the viewpoint of our specific task it is important that the described procedure gives the value of the material parameter

$$\lambda \equiv \sigma/k_c \tag{14}$$

With the value of λ thus obtained, and with $k_c = 1.8 \times 10^{-19}$ J [42], we calculate the membrane tension σ from Eq. (14) and the adhesion energy per unit area from the expression

$$w_a = \lambda k_c(1 - \cos\theta_h) \tag{15}$$

cf. Eq. (3). Finally, the total adhesion energy of the cell is computed:

$$W_a = \pi r_f^2 w_a \tag{16}$$

In this way the goal of our study is, in principle, achieved. The results are reported in the next section.

It should be noted that the predictions of Eq. (12), concerning the possible shapes of a free (non-adherent) closed membrane, characterized with tension σ and bending elasticity k_c, are not examined. Our preliminary numerical calculations, based on the procedure from Appendix C, show that Eq. (12) predicts a transition in the shape of the membrane from a 'spherocyte' to a biconcave 'discocyte' with the increase of osmolarity; the latter is characterized by the pressure difference ΔP. In other words, it turns out that a

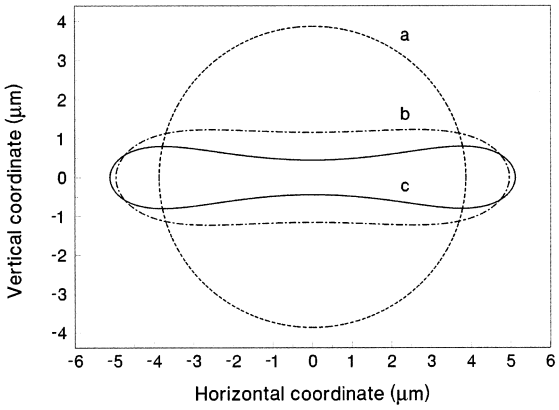

Fig. 6. Shape of a closed membrane calculated by means of Eq. (12) for $k_c = 1.8 \times 10^{-19}$ J and for fixed membrane area $A_T = 188$ μm^2. (a) spherocyte; (b) discocyte corresponding to $\sigma = 1.8 \times 10^{-4}$ mN/m and $\Delta P = 0.036$ Pa; (c) discocyte corresponding to $\sigma = 3.6 \times 10^{-4}$ mN/m and $\Delta P = 0.072$ Pa.

membrane with non-zero bending elasticity, k_c, can acquire 'discocyte' shape even with zero shear elasticity. In our computations we fixed the values of the total membrane area A_T and the bending elasticity k_c, whereas ΔP and σ were varied. As an illustration Fig. 6 shows two 'discocyte' profiles, corresponding to some specific values of σ and ΔP given in the figure caption, compared with the spherical shape of the same 'cell'. A complete survey demands a phase diagram of all possible cell configurations in the $(\sigma, \Delta P)$-plane to be built up. However, this task is beyond the scope of the present paper and could be a subject of a separate study.

4. Results and discussion

4.1. Results for native erythrocytes

First we processed the interference pattern produced by two adherent native (untreated) erythrocytes at four different values of the solution osmolarity: 143, 151, 153 and 156 mOsm. Hypotonic Tris-buffer solutions are used, which contain 4.5×10^{-2} M NaCl at four different concentrations of sucrose. The results obtained for the two cells turned out to be very similar. In Table 1 we give the mean values of $2R$, $2r_f$ and θ_h for these two cells. The values of R are obtained from the best fits of $H_k^2 + r_k^2$ vs. H_k, as explained in Section 3.1 (Fig. 5). We recall that the radii of the interference rings, r_k, are determined by averaging over the measurements along four different radial sections of the interference pattern from the cell (cf. Fig. 3). The values of θ_h are computed with the help of Eq. (7). The standard error of R (in average $\Delta R \approx 0.3$ μm) is obtained from the error of the slopes and the intercepts of the linear regressions, like those in Fig. 5. The standard error of the directly measured diameter, $2r_f$, ($2\Delta r_f \approx 0.2$ μm) in fact is determined by the limit of the microscope resolution ability; the standard error of θ_h is calculated from ΔR and Δr_f.

The data in Table 1 show that $2r_f \approx 1.7$ μm is practically constant irrespective of the variation of osmolarity. This means that the area of adhesive contact, initially formed at osmolarity 143 mOsm, remains practically constant when the osmolarity is increased up to 156 mOsm. The degree of erythrocyte swelling decreases with the increase of osmolarity, which makes the membrane more flaccid and leads to decrease of the membrane

Table 1
Average data for two similar untreated erythrocytes attached to a glass surface at 20°C for various osmolarities, C_{osm}

C_{osm} (mOsm)	$2R \pm 0.3$ (μm)	$2r_f \pm 0.2$ (μm)	$\theta_h \pm 1.7$ (deg)	λ (1/μm^2)	w_a 10^{-8} J/m^2	σ^a 10^{-4} mN/m	ΔP^a (Pa)	$\frac{W_a}{kT}^a$
143	7.8	1.7	12.5	–	–	4.9	0.25	6.4
151	6.7	1.6	13.9	2.2	1.16	4.0	0.24	5.7
153	6.8	1.7	14.3	2.1	1.17	3.7	0.22	6.4
156	5.8	1.7	17.4	1.4	1.15	2.5	0.17	6.4

[a] The quantity is calculated using the average value $w_a = 1.16 \times 10^{-8}$ J/m^2.

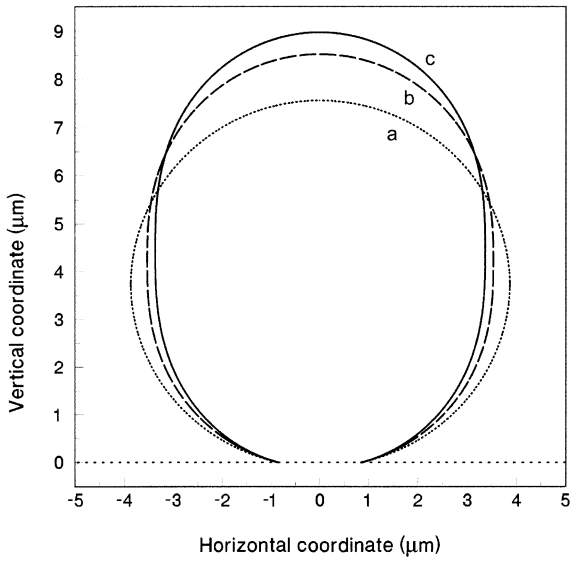

Fig. 7. Shape of an erythrocyte adherent to a glass substrate; the zone of the flat adhesion film is in the lower part of the graph. (a) For $C_{osm} = 143$ mOsm the non-adherent membrane is assumed to be spherical; the shape for (b) $C_{osm} = 153$ mOsm and (c) $C_{osm} = 156$ mOsm is reconstructed from the data in Table 1 by solving Eq. (12); k_c and A_T are the same as in Fig. 6.

tension, σ. As noted in Section 2.1, there are two regimes of membrane dilatation: (i) apparent stretching (flattening of the thermally-excited undulations of a flaccid membrane) and (ii) direct elastic stretch. Since the lysis occurs at $C_{osm} = 135$ mOsm, one can estimate that the regime of direct elastic stretch takes place at $135 < C_{osm} < 139$ mOsm, whereas the regime of apparent stretching takes place for $C_{osm} > 139$ mOsm. Therefore, all data in Table 1 correspond to the regime of apparent stretching (flaccid membrane). In this regime the values of the relative membrane dilatation α and the membrane tension σ are expected to be rather low [23].

If the shape of an adherent cell was truncated sphere, then the total area of the cell membrane could be calculated from the equation

$$A_T = 2\pi R^2(1 + \cos\theta_h) + \pi r_f^2 \quad (17)$$

Using Eq. (17) and the parameters values in Table 1 one calculates that the membrane area varies from $A_T = 188$ μm^2 for $C_{osm} = 143$ mOsm down to $A_T = 107$ μm^2 for $C_{osm} = 156$ mOsm. Such a large calculated variation of the membrane area (with 31%) could be attributed neither to elastic shrinking, nor to thermal surface undulations. The only acceptable explanation of the latter finding is that the shape of the flaccid membrane deviates from sphere. In fact, thanks to this deviation from sphericity we can determine the membrane tension, σ, and the energy of cell adhesion, w_a, with the help of the generalized Laplace Eq. (12), as explained in Section 3.2 and Appendix C. In this aspect, our approach to the calculation of the membrane tension σ resembles the pendant drop method for measuring static interfacial tension, which employs the common Laplace equation of capillarity (see, e.g. [43,44]).

To specify the value of the total membrane area A_T, needed in the boundary condition (v) in Section 3.2, we assume that at osmolarity $C_{osm} = 143$ mOsm the erythrocyte is spherical and then its area is $A_T = 188$ μm^2, as calculated from Eq. (17) with the values of R and r_f for 143 mOsm in Table 1. Then it is accepted that the area is (approximately) the same, $A_T \approx 188$ μm^2, for the other osmolarities (151, 153 and 156 mOsm), insofar as the membrane dilatation is expected to be rather low, $\alpha \ll 1$. Next, Eq. (12), along with Eq. (10), is integrated numerically. The solution, corresponding to a set of values of the geometrical parameters R, r_f, θ_h, and A_T, is uniquely determined. As a result of integration we obtain the respective values of the parameter λ (Eq. (14)) which are listed in Table 1.

The profiles of the adherent erythrocyte, calculated by means of the numerical integration (Appendix C) are depicted in Fig. 7 for $C_{osm} = 143$, 153 and 156 mOsm; the deviation from the sphericity increases with the rise of osmolarity. The profile for $C_{osm} = 151$ mOsm (not shown in Fig. 7) is very close to that for $C_{osm} = 153$ mOsm. The shape of the attached non-spherical erythrocytes somewhat resembles a prolate ellipsoid of revolution. It should be noted, that the calculated shape in the lower part of the adherent erythrocytes (in the zone where the interference fringes appear) turns out to be really close to spherical, i.e. the local values of the two principal curvatures are almost equal, $c_1 \approx c_2$. This finding is conso-

nant with our procedure of determination of R, r_f and θ_h by a local fit of the data from the interference fringes with a spherical profile, Eq. (6); this procedure is also justified by the good agreement of the data in Fig. 5 with the theoretical lines.

Next, from the values of θ_h and λ, listed in Table 1, we compute w_a using Eq. (15) with $k_c = 1.8 \times 10^{-19}$ J [42]. The obtained values of w_a for the three solution osmolarities, $C_{osm} = 151$, 153 and 156 mOsm, are very close to each other (Table 1). Hence, the increase of osmolarity by addition of sucrose practically does not affect the forces, which are responsible for the erythrocyte adhesion to the substrate. Then the variation of the contact angle θ_h can be attributed entirely to the variation of the membrane tension σ with osmolarity at fixed w_a (Eq. (3)). Indeed, the rise of osmolarity decreases the swelling of the erythrocyte, makes its membrane more flaccid and decreases its tension σ. To quantify the latter tendency we took the average value of w_a (Table 1),

$$w_a = 1.16 \times 10^{-8} \text{ J/m}^2, \quad \text{(untreated erythrocytes)} \tag{18}$$

and then calculated the membrane tension from the expression $\sigma = w_a/(1 - \cos\theta_h)$. The computed σ's are listed in Table 1. One sees that membrane tension σ is really very low (of the order of 10^{-4} mN/m) and decreases with the rise of osmolarity, as it should be expected.

Further, from the values of R and σ in Table 1 we calculate the pressure difference across the erythrocyte membrane, $\Delta P = 2\sigma/R$; the values of ΔP thus obtained are listed in the table. We recall that the usage of Eq. (13) is justified because in the zone of the interference fringes the membrane profile can be locally approximated with a sphere of radius R (Fig. 5 and Eq. (6)). As it could be expected, ΔP decreases with the increase of osmolarity, despite the decrease of the curvature radius R (Table 1).

Finally, by means of Eqs. (16) and (18) we estimate the total adhesion energy, W_a, which is about $6.4kT$ (Table 1), where k is the Boltzmann constant and T is the temperature. This value of W_a is larger than the thermal energy, kT, and is consonant with the fact that the Brownian motion does not detach the adherent erythrocytes from the glass substrate. Dolowy [6] has estimated a somewhat larger erythrocyte adhesion energy: $W_a \approx 30kT$; the difference could be attributed to the fact that in our case the cells are swollen and the contact area is smaller.

The value $W_a \approx 6.4kT$ is rather low to be due to some specific interactions, such as chemical bonds (which, by the way, are not expected for erythrocyte–glass contact). There are at least two possible explanations about the physical origin of the adhesion energy. (i) It can be attributed to the van der Waals attraction across the aqueous film in the multilayered system glass/water/cell-membrane/cell-interior. Estimations based on the known Hamaker formula [45] show that the van der Waals attraction could explain the observed adhesion if the electrostatic repulsion is completely disregarded. (ii) The adhesive energy can also be attributed to the short-range electrostatic attraction due to the discreteness of the surface charge. The theory of the latter effect, developed by Richmond [46,47], brings into agreement the measured and the calculated adhesion energies in black Newtonian films [48]. The experiments with trypsin treated cells described in the next subsection helps to discriminate between the above two possible explanations of the origin of cell-to-glass adhesion.

4.2. Erythrocytes treated with trypsin

The treatment of erythrocyte membrane with trypsin leads to a detachment of some hydrophilic fragments from the membrane glycoproteins [17]. This leads to a decrease of the surface charge density up to three times as established by means of electrophoretic measurements [18,49]. We followed the procedure for trypsin-treatment described by Wolf and Gingell [17]. Erythrocytes, washed after centrifugation, were resuspended in isotonic trypsin solution (Appendix A) and incubated within 1 h at 37°C. Then the erythrocytes were separated by centrifugation and washed twice with isotonic buffer solution. For the adhesion experiments a stock erythrocyte suspension of cell volume fraction 50% was obtained by

resuspending of trypsin treated erythrocytes in hypotonic buffer with osmolarity of 143 mOsm.

To reveal whether the reduction of the erythrocyte surface charge by the trypsin has some impact on the adhesion properties, we carried out experiments analogous to those with the untreated (native) cells. The results for three examined erythrocytes at osmolarities $C_{osm} = 143$, 151 and 153 mOsm at 20°C are listed in Table 2. The values of the measured parameters are given separately for each cell, without averaging. Thus the data demonstrate the individual differences between the cells. The geometrical parameters R, r_f and θ_h are determined from the interference pattern as described in Section 3.1.

The membrane tension, σ, and W_a of the trypsin treated erythrocytes have been estimated in the following way. It is reasonable to accept that the trypsin modifies only the outer surface of the cell membrane, but it does not alter the cell interior. In such a case the difference in ΔP, must be the same for native and trypsin treated erythrocytes if only the temperature and the osmolarity of the outer medium are the same. Then we can use the values of ΔP from Table 1 to calculate σ in Table 2 for the respective values of R and osmolarities by using Eq. (13). One sees that the results for σ thus obtained (Table 2) are close to the respective values in Table 1, although there are differences between the individual cells. Next, we calculate w_a and W_a by means of Eqs. (3) and (16) using the values of r_f, θ_h and σ from Table 2. The average value of the adhesion energy for the trypsin-treated cells, $W_a \approx 4.5kT$ is lower than the average value $6.2kT$ obtained for the native cells (cf. Tables 1 and 2). The calculated average adhesion energy per unit area,

$$w_a = 0.98 \times 10^{-8}\ \mathrm{J/m^2},$$
(trypsin-treated erythrocytes) (19)

is also smaller than the respective value for untreated cells (cf. Eqs. (18) and (19)). Similar indications about a lower adhesion ability of trypsin treated erythrocytes have been obtained by Wolf and Gingel [17]. This difference between treated and untreated cells cannot be explained by the van der Waals attractive forces, which are not sensitive to the surface charge density. Moreover, at a first glance the decrease of adhesion with the reduction of the surface charge (by the trypsin treatment) could seem surprising, because the decrease of the electrostatic repulsion allows the adhesive surface forces (such as the van der Waals interaction) to show up. In contrast, the short-range electrostatic attraction, due to the discreteness of the surface charge, decreases with the decrease of the surface charge density [46,47,50,51], which is consonant with the observed weakening of erythrocyte adhesion owing to the trypsin treatment. Consequently, the established effect of trypsin on the adhesion energy indicates that in this case the adhesion could

Table 2
Data for the attachment of trypsin-treated erythrocytes to a glass surface at 20°C for various osmolarities, C_{osm}

C_{osm} (mOsm)	$2R \pm 0.3$ (μm)	$2r_f \pm 0.2$ (μm)	$\theta_h \pm 1.7$ (deg)	$\sigma\ 10^{-4}$ mN/m	$\frac{W_a}{kT}$
143					
Cell 1	7.0	1.4	11.5	4.4	3.3
Cell 2	7.8	1.6	11.8	4.9	5.1
151					
Cell 1	6.8	1.4	12.3	4.1	3.5
Cell 2	7.9	1.7	12.4	4.7	6.1
Cell 3	6.4	1.5	13.9	3.8	4.8
153					
Cell 1	7.1	1.5	12.2	3.9	3.8
Cell 2	8.4	1.6	11.1	4.6	4.2
Cell 3	7.0	1.6	13.5	3.8	5.1

Table 3
Data for the adhesion of untreated and glycophorin-treated erythrocytes to a glass substrate at 37°C and osmolarity $C_{osm} = 153$ mOsm

Erythrocyte	Cell number	$2R$ (μm)	$2r_f$ (μm)	θ_h (deg)
Untreated with glycophorin	1	9.6	1.4	8.6
	2	8.3	1.3	9.0
	3	7.6	1.2	9.3
Treated with glycophorin	1′	6.0	0.3	2.3
	2′	7.7	1.0	7.0
	3′	5.7	0.8	7.9

originate from this short-range electrostatic attraction. The latter, in combination with the van der Waals interaction, can prevail over the double-layer repulsion.

4.3. Erythrocytes treated with glycophorin

In contrast with the trypsin treatment, the treatment with glycophorin increases the surface charge density of erythrocytes (see Appendix B for details about the experimental procedure). The glycophorin is an integral membrane protein, which is naturally contained in the erythrocyte membrane (c.a. 500 000 molecules per cell), and which bears a negative electric charge. We incorporated additional amount of glycophorin in the cell membrane following the procedure developed by Arvinte et al. [52]. Fluorescence measurements (Appendix B) show that in this way we have achieved a 5.5 times increase of the glycophorin contents in the membrane, which is expected to cause a considerable rise of the surface electric charge.

Preliminary experiments [53] indicated that the additional amount of glycophorin in the cell membrane makes the erythrocyte-to-glass adhesion more difficult. It was found that the adhesion is favored by the rise of both temperature and osmolarity [54]. For that reason, to achieve adhesion of glycophorin-treated erythrocytes to the substrate, we worked at a higher temperature, 37°C, and at a not-too-low osmolarity, 153 mOsm. The observations showed that under these experimental conditions erythrocytes without additionally incorporated glycophorin in their membrane give interference patterns with a dark central spot, but very often without completely circular symmetry. This means that the adhesive films are relatively thin, the membrane is rather flaccid, and the erythrocyte shape is not spherical. In contrast, the attached erythrocytes with additionally incorporated glycophorin give interference pattern with circular symmetry and with a significantly brighter central spot. This is evidence of a higher membrane tension and lower adhesion energy of the glycophorin-treated erythrocytes.

The above qualitative observations were confirmed by the quantitative results from the reflection interference microscopy. Table 3 contains results for three native and three glycophorin-treated erythrocytes at temperature 37°C. The values of $2R$, $2r_f$, and θ_h are determined in the same way as described in Section 3.1. The values of $2r_f$ and θ_h in Table 3 for the treated cells are markedly smaller than these for the untreated cells. The latter fact clearly indicates weaker adhesion of the glycophorin treated cells.

Unfortunately, we do not have data for the area of the glycophorin-treated erythrocytes; this would allow us to calculate their membrane tension and adhesion area, just like we did in Section 4.1 above. We cannot use the values of ΔP in Table 1, because they are determined at a lower temperature (20 rather than 37°C) and the Donnan equilibrium is sensitive to variations in temperature. In future experiments we plan to determine the area of glycophorin treated cells by decreasing the osmolarity and measuring the diameter of the obtained spherocytes. This would enable us to extract the full information from the

interference fringes, as we did for the untreated cells (Table 1).

5. Concluding remarks

In the present work we studied the adhesion of osmotically swollen erythrocytes to glass substrates. An experimental chamber was used (Fig. 2), which allowed us to observe the cell adhesion and to vary the osmolarity of the medium around the adherent erythrocytes. We carried out measurements with the same cell at various compositions of the medium thus detecting the influence of individual cell properties (age, size, charge, etc.). In our experiments the osmolarity was varied between 143 and 156 mOsm; the erythrocytes looked spherical in the bulk of these hypotonic solutions. The swelling of the cells and their σ increase with the decrease of osmolarity. In this osmolarity range the membrane stretching (due to swelling) happens in the regime of flaccid membrane, through flattening (suppression) of thermally excited undulations (Section 4.1).

The cells attached to a glass substrate in the experimental chamber produce interference pattern (Newton rings) when observed in reflected light, see Fig. 3. The interference pattern has been recorded by means of a video camera and then processed by computer to obtain information about the profile of the cell in the zone of adhesive contact with the substrate (Fig. 4, Tables 1–3). The area of an attached cell can be determined by measuring the curvature radius of the swollen cell at lower osmolarity, at which the non-adherent part of the cell membrane is spherical.

At higher osmolarities the non-adherent part of the cell membrane acquires a slightly elongated shape (Fig. 7). This deviation from sphericity enables one to determine the membrane tension σ with the help of a method, proposed in Section 3.2, which somewhat resembles the pendant-drop method in interfacial tensiometry. The generalized Laplace equation, which accounts for the bending elasticity of the membrane, k_c, is solved numerically along with appropriate boundary conditions; the necessary values of some geometrical parameters are extracted from the interference data. The mathematical problem has a unique solution, which gives the value of the membrane tension σ for each given axisymmetric configuration of an adherent cell, supposedly the membrane bending elasticity k_c is known. From the determined value of σ we calculate the pressure drop across the membrane of the swollen cell and the energy of adhesion between the cell and the glass substrate (Tables 1 and 2).

To reveal the physical origin of the observed cell-to-glass adhesion we carried out experiments with (i) untreated (native) erythrocytes, with (ii) trypsin-treated erythrocytes having lower surface electric charge and (iii) with glycophorin-treated erythrocytes having higher surface electric charge. The comparison of the determined adhesion energies for untreated and trypsin-treated erythrocytes indicates that the adhesion could be attributed to the action of the short-range electrostatic attraction due to the discreteness of the surface charge (Section 4.2).

The experiments with the glycophorin-treated erythrocytes show that at 20°C there is no cell-to-glass adhesion at all, whereas at 37°C adhesion is observed, but it is weaker than for untreated cells (Section 4.3). The latter findings can be explained with the electrostatic double layer repulsion, which is enhanced by the incorporation of additional electrically charged glycophorin molecules in the cell membrane.

We hope that the developed mathematical and numerical procedure for solving the generalized Laplace equation (Appendix C) can find application for interpreting the configurations of closed biological and model membranes (vesicles) and can bring information about the physical parameters of the system, such as membrane tension, difference in pressure or electric potential across the membrane, its bending elasticity and spontaneous curvature, adhesion energy, etc. As a side result we established that the generalized Laplace equation (without shear elasticity) predicts a transition in the shape of a closed membrane from a 'spherocyte' to a biconcave 'discocyte' with the increase of osmolarity (Fig. 6). A phase diagram of all possible cell configurations predicted by this equation could be a subject of a subsequent study.

Acknowledgements

The support from the Franco-Bulgarian Laboratory 'Vesicles and Membranes' is gratefully acknowledged.

Appendix A. Solutions used in the experiments

Isotonic Tris-buffer solution with pH = 7.4 was prepared at 20°C from 0.145 M NaCl (p.a. grade, from Fluka), 0.0147 M Trizma HCl and 0.0023 M Trizma base (products of Sigma, St Louis, MO).

Hypotonic Tris-buffer solutions: the value of pH affects the physiological state and the lysis of erythrocytes. Our experiments are carried out at pH = 7.4 and at two different temperatures, 20 or 37°C. As known, the pH of Tris-buffers depends strongly on temperature. For this reason two types of hypotonic Tris-buffered solutions with 4.5×10^{-2} M NaCl were prepared in order to obtain the same pH = 7.4 at the respective temperatures:

1. Solutions of various osmolarities, 143, 151, 153 and 156 mOsm, (1 mOsm = 1 mM total concentration of dissolved ions and non-dissociated species) were used. This was achieved by varying the concentration of sucrose (from Merck). pH = 7.4 at 20°C in these solutions was obtained by using 0.0147 M Trizma HCl and 0.0023 M Trizma base.
2. Solution of pH = 7.4 at 37°C was prepared by dissolving 0.0123 M Trizma HCl and 0.00466 M Trizma base. Solution with osmolarity 153 mOsm was obtained by adding 0.0236 g sucrose.

Sodium acetate buffer solutions with various pH: 3.75, 4.05, 4.27, 4.60, 4.80 and 4.99, at constant osmolarity, 290 mOsm, were used in the procedure of glycophorin incorporation into the erythrocyte membrane (Appendix B). These solutions were prepared by mixing 0.02 M CH_3COOH and 0.02 M CH_3COONa in various volume ratios. The pH of all solutions was measured by a pH-meter (HI9314000, Hanna Instruments).

Sodium carbonate buffer solution with pH = 9.5 and osmolarity of 290 mOsm was used in the experiments for labeling of glycophorin molecules with the dye fluorescein isothiocyanate (FITC), see below. This buffer was prepared by mixing of 50 ml of 0.05 M Na_2CO_3, 5.0 ml of 0.05 M HCl and an amount of NaCl needed to achieve the physiological osmolarity.

Trypsin solution: it was prepared by solving of 10 μg of the enzyme trypsin in 1 ml isotonic buffer with pH = 7.4. The used trypsin was from bovine pancreas-type 3 (Sigma).

FITC solution: a stock solution of 4.0 mg FITC-isomer 1 (Sigma) in 1 ml sodium carbonate buffer was prepared. The solution was stored in a dark container. It was used for labeling of glycophorin and for preparing of diluted solutions of FITC with the following concentrations: 6.5×10^{-6}, 3.27×10^{-6}, 1.64×10^{-6} and 6.55×10^{-7} M. Based on the measured absorption spectra of these solutions at $\lambda = 280$ and 490 nm calibration curves of FITC were obtained. From the slopes of these curves we determined the FITC absorbancies, $a_{280} = 40.62$ cm^2/mg and $a_{490} = 205.30$ cm^2/mg, at the respective wavelengths. The latter two parameters were used for calculating the concentration of the labeled glycophorin.

Glycophorin solution*:* we used glycophorin from human blood-type MM (predominantly glycophorin A), product of Sigma. A stock isotonic solution of glycophorin with concentration 0.5 mg/ml was prepared; 0.9 ml of this solution was labeled with FITC. The rest of the stock solution was used for preparing of isotonic diluted glycophorin solutions with the following concentrations: 0.007 mg/ml, 0.014 mg/ml and 0.028 mg/ml. Their absorption spectra were recorded at $\lambda = 280$ nm. Thus a calibration curve was obtained and from its slope the absorbancy of glycophorin was determined to be $a_{280} = 1.23$ cm^2/mg.

All solutions were prepared with triply distilled water.

Appendix B. Glycophorin treatment

Our purpose is to incorporate an additional amount of the membrane protein glycophorin into the membrane of erythrocytes. For that purpose we utilize and extend the procedure developed by Arvinte et al. [52].

(i) Labeling of the glycophorin with a fluorescence marker. FITC was used for this purpose. FITC bounds covalently to the terminal amino-group of the lysine fragment in the protein molecule. To satisfy the requirements for optimal conditions (temperature and pH), the labeling was carried out in alkaline medium at room temperature (25°C) within 1.5 h in a mixture of 0.9 ml isotonic solution of glycophorin and 0.1 ml FITC solution (pH = 9.5) (see Appendix A about the composition of the respective solutions).

(ii) Chromatographic separation of the labeled glycophorin. The complex FITC–glycophorin was separated from the non-reacted FITC in the solution by a molecular sieve chromatography. The column used by us had dimensions 24×1 cm. Sephadex G-25 (product of Pharmacia Fine Chemicals, Sweden) was used as a stationary phase and isotonic Tris-buffer (pH = 7.4) as a mobile phase. The column had been filled up with gel (2.7 g Sephadex and 50 ml isotonic buffer) and equilibrated with 100 ml isotonic Tris-buffer solution (passed through the column with a flow rate of 30 ml/h). Then 400 μl of the FITC–glycophorin mixture were carefully delivered by a pipette. The elution phase was collected as fractions with a volume of 2 ml. Because of the high molecular weight of the glycophorin, the complex FITC–glycophorin was running out of the column with the so called 'void' volume, while the remaining unbound FITC was eluted with the 'bed' volume. The elution rate was 40 ml/h. In this way the whole amount of the FITC–glycophorin complex has been collected in a small volume (4 ml) in the very beginning of the elution process. On the other hand, the free FITC left the column slower, after 15 ml of the elution liquid had been already collected.

(iii) Determining the concentration of the FITC–glycophorin complex. The concentration of the complex, C_{Gl}, and that of the bound FITC, C_{FITC}, were determined in the following way [52]. We measured the absorptions, A_{280} and A_{496}, of the FITC–glycophorin complex at $\lambda = 280$ and 496 nm respectively. From independent measurements we knew the absorbancies, $a_{280} = 40.62$ cm^2/mg and $a_{490} = 205.30$ cm^2/mg, of pure FITC in solution determined from calibration plots (Appendix A). Then we calculated C_{Gl} and C_{FITC} using the following equations [52]:

$$C_{Gl} = \frac{A_{280} - (0.36 \times A_{496})}{a_{280}} \quad (20)$$

$$C_{FITC} = \frac{A_{496}}{a_{490} \times 0.75} \quad (21)$$

Because of simultaneous manifestation of batochromic and hypochromic effects the long-wave absorption maximum of bound FITC is at 496 nm. Its absorbancy is 0.75 from the absorbancy of unbound FITC [55]. The ratio of the FITC absorptions at 280 and 496 nm is in the range between 0.35 and 0.38 [55]. The multiplier 0.36 in Eq. (20) is a correction that accounts for the FITC absorption at 280 nm. The concentrations of labeled protein and the bound FITC thus calculated are $C_{Gl} = 9.68 \times 10^{-7}$ M and $C_{FITC} = 3.33 \times 10^{-7}$ M. Since $C_{Gl}/C_{FITC} = 2.9$, one can conclude that (approximately) each third glycophorin molecule is labeled by one FITC molecule.

(iv) Incorporation of the FITC–glycophorin complex in the erythrocyte membrane. To do that we used the low-pH method [52]. As experimentally established, when erythrocytes are put in a medium with pH < 5.4, point defects appear in their membranes. These defects can further grow and form channels. If a protein, inherent for the cell, is present in the medium, it can incorporate in these channels thus protecting the cell from lysis. The extent of the defect growth depends on pH and the temperature of the medium. We experimentally found out that the lysis of the used erythrocytes is the fastest when the cells are resuspended in a medium with pH = 3.6 or 4.0. If pH is > 4.6 the process of lysis is slowed down and takes about a couple of hours.

In the present study the incorporation of glycophorin is performed in isotonic sodium acetate buffer with pH = 4.0 at 37°C. The procedure is the following. We add 0.028 ml isotonic erythrocyte suspension, containing 2.8×10^7 cells, to a mixture of 2.69 ml isotonic acetate buffer and 0.318 ml solution of the FITC–glycophorin complex with concentration 9.68×10^{-7} M. The obtained mixture is incubated for 2 min. Then the

erythrocytes are separated by centrifugation, washed with isotonic buffer and stored for the adhesion experiments. The percentage of the incorporated glycophorin is determined spectrofluorimetrically based on the fluorescence emission intensity at wavelength $\lambda_{em} = 514$ nm, the excitation wavelength being $\lambda_{ex} = 470$ nm. The changes in the fluorescence intensity are recorded by a Perkin–Elmer LS-3 fluorescence spectrometer. Fig. 8A presents the fluorescence emission spectra of the FITC–glycophorin complex before (curve 1) and after (curve 2) the mixing with the erythrocytes at pH = 4.0. At the end of this experiment we added to the erythrocyte suspension a solution of the nonionic surfactant Triton X-100 (product of Fluka) with final concentration 1%. This surfactant solubilizes all proteins and lipids into micelles, offering to FITC-labeled proteins a hydrophobic environment similar to that of the membrane, which leads to a strong reducing of the emission peak at $\lambda_{em} = 514$ nm (curve 3 in Fig. 8A).

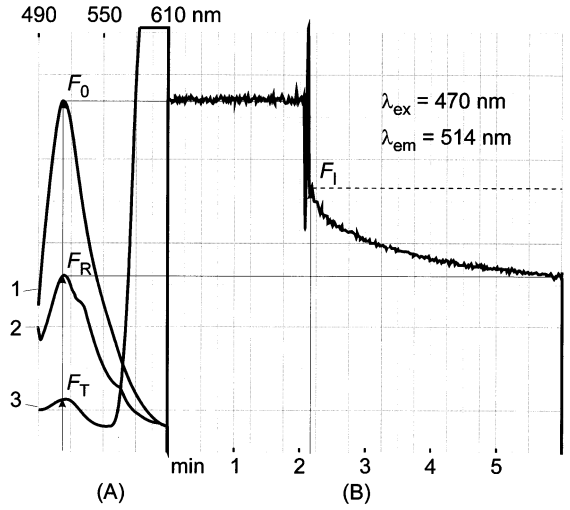

Fig. 8. (A) Emission spectrum of the FITC–glycophorin complex before (curve 1) and after (curve 2) the addition of erythrocytes at pH = 4.0; curve 3 shows the spectrum after the addition of Triton X-100. (B) Time dependence of the fluorescence intensity at $\lambda_{em} = 514$ nm: F_0 and F_I are the intensities before, and immediately after, the addition of erythrocytes; F_R is the intensity after the equilibration of erythrocytes and glycophorin.

Fig. 8(B) shows the experimental time-dependence of the fluorescence intensity at $\lambda_{em} = 514$ nm. One observes a sharp drop of the intensity at the moment, when the erythrocyte suspension is added to the solution of the FITC–glycophorin complex. This observation can be explained with the filter effect of the added concentrated cell suspension. Next, the fluorescence intensity gradually decreases, beginning from an initial value, F_I, down to an equilibrium value F_R (Fig. 8B). The latter process evidences for the incorporation of the FITC–glycophorin complex into the erythrocyte membranes, which is completed within 5 min. Using the measured values of the fluorescence intensities the percentage of the incorporated glycophorin was calculated by means of the following equation:

$$C_{\%} = \left(\frac{F_I - F_R}{F_I - F_T}\right) \times 100 \ (\%) \tag{22}$$

Here F_T is the fluorescence from the sample at $\lambda_{em} = 514$ nm after treatment with Triton X-100. Thus from the data in Fig. 8 one obtains $C_{\%} = 41\%$. Knowing the concentrations of glycophorin and erythrocytes we estimated that the procedure described above leads to the incorporation of 2.7×10^6 glycophorin molecules in every erythrocyte. This amount is almost 5.5 times greater than the amount of the native glycophorin in the erythrocyte membrane.

Appendix C. Solution of the generalized Laplace equation

It is convenient to introduce the auxiliary function

$$F \equiv \frac{\mathrm{d}\sin\theta}{\mathrm{d}r} + \frac{\sin\theta}{r} - \frac{2}{b}, \qquad b \equiv \frac{2\sigma}{\Delta P} \tag{23}$$

where b is constant if the effect of gravity on the erythrocyte shape is negligible. Then the generalized Laplace equation, Eq. (12), acquires the form

$$\frac{\cos\theta}{r}\frac{\mathrm{d}}{\mathrm{d}r}\left(r\cos\theta\frac{\mathrm{d}F}{\mathrm{d}r}\right) = \lambda F \tag{24}$$

where λ is defined by Eq. (14). We will use as an independent variable the length of the generatrix

of the membrane profile, s, whose differential is related to the differentials of the cylindrical coordinates (r, z) as follows:

$$dr = \cos\theta\ ds, \qquad dz = \sin\theta\ ds \tag{25}$$

The introduction of s as a variable of integration helps to avoid divergence in the procedure of numerical integration at the 'equator' of the erythrocyte, where $\cos\theta = 0$. The differential of the membrane area, A, is simply related to ds:

$$dA = 2\pi r\, ds \tag{26}$$

Combining Eqs. (23) and (25) one obtains

$$\frac{d\theta}{ds} = \frac{2}{b} - \frac{\sin\theta}{r} + F(s) \tag{27}$$

Likewise, from Eqs. (24) and (25) one derives

$$\frac{d^2F}{ds^2} = \lambda F - \frac{|\cos\theta|}{r}\frac{dF}{ds} \tag{28}$$

Eqs. (25)–(28) form a set of five equations for determining the five unknown functions $r(s)$, $z(s)$, $\theta(s)$, $F(s)$ and $A(s)$. In particular, the functions $r(s)$ and $z(s)$ determine the profile of the axisymmetric membrane in a parametric form.

Let us now apply the set of Eqs. (25)–(28) to determine the profile of the adherent erythrocyte from the data in Table 1. We start the numerical integration from the apex of the membrane surface, i.e. from the upper point of the profiles in Fig. 7, where the generatrix intersects the axis of revolution. We set $s = 0$ at this point. Eqs. (25)–(27) are ordinary differential equations. Therefore, each of them needs one boundary condition; in our case these are:

$$r(s=0) = 0; \qquad z(s=0) = 0;$$
$$\theta(s=0) = 0 \quad \text{and} \quad A(s=0) = 0 \tag{29}$$

It is an experimental finding that the membrane profile in the zone of the interference fringes can be approximated with a sphere of radius R (Section 3.1). Then in Eq. (27) one can set $b = R$; the values of R are listed in Table 1 for various osmolarities. Finally, the two boundary conditions for Eq. (28) are:

$$F(s=0) = q \quad \text{and} \quad \frac{dF}{ds} = 0 \quad \text{for} \quad s = 0 \tag{30}$$

The latter boundary condition removes a divergence in Eq. (27) for $s = 0$ ($r = 0$). On the other hand, q is an unknown parameter, which is to be determined, together with the other unknown parameter λ, from the area of the free (non-adherent) portion of the membrane:

$$A_F = A_T - \pi r_f^2 \tag{31}$$

where A_T (in this case 188 μm^2) is the total area of the membrane, assumed constant; the experimental values of r_f are given in Table 1. Then the two unknown parameters, q and λ, are to be determined from the following two conditions:

$$r = r_f \quad \text{and} \quad \theta = \theta_h \quad \text{for} \quad A = A_F \tag{32}$$

The experimental values of θ_h are also given in Table 1.

To obtain the profiles of adherent cells shown in Fig. 7 we started the integration from the membrane apex, $s = 0$, with tentative values of the unknown parameters, q and λ. Further, the integration continues until we reach the point with $A = A_F$. Then we check whether Eq. (32) is satisfied. If not, we assign new values of q and λ and start the integration again from the apex $s = 0$. This continues until we find such values of q and λ, which lead to fulfilment of Eq. (32). These values can be automatically determined by numerical minimization of the function

$$\Phi(q,\lambda) = [r(A_F;q,\lambda) - r_f]^2 + [\theta(A_F;q,\lambda) - \theta_h]^2 \tag{33}$$

with respect of q and λ. Thus we determined the values of λ, which are listed in Table 1.

The curves in Fig. 6 illustrate what would be the shape of the same erythrocyte (of the same area $A_T = 188$ μm^2) if it were not attached to the substrate. In other words, Fig. 6 shows the shape of a free (non-attached) erythrocyte of area $A_T = 188$ μm^2 at various values of the membrane tension σ and the transmembrane pressure difference ΔP, specified in the figure caption. The curves in Fig. 6 are also obtained by numerical integration of Eqs. (25)–(28). As before, the integration starts from the apex of the profile, i.e. from the intersection point of the generatrix with the axis of revolution, where we set $s = 0$. The values of λ and b are known, since the values of σ, ΔP and k_c are

given, see Eqs. (14) and (23). The numerical integration starts with a tentative value of q in Eq. (30). The value of q is determined from the condition that when the integration reaches the membrane 'equator', where $\cos\theta = 0$, the membrane area must be $A = A_T/2$.

Since the membrane profile is symmetric with respect to the 'equatorial' plane, we carry out the numerical integration above the equator, and then we obtain the profile below the equator as a mirror image. Of course, one can continue the numerical integration after crossing the equator and the same profile will be obtained; however, due to accumulation of error from the numerical procedure this could decrease the accuracy of the calculated profile for the higher values of s (below the equator).

Our calculations indicated that the generalized Laplace equation, Eq. (12), or the equivalent set of Eqs. (25)–(28), has at least two types of solutions for a free (non-adherent) erythrocyte of fixed area and given membrane tension σ. The first type is a discocyte like those in Fig. 6. The second type looks like an oblong ellipsoid of revolution, which resembles the shape of a red blood cell penetrating along a narrow capillary.

References

[1] P. Bongrand, Intermolecular forces, in: P. Bongrand (Ed.), Physical Basis of Cell–Cell Adhesion, CRC Press, Boca Raton, FL, 1988.
[2] V.A. Parsegian, D. Gingell, J. Cell Sci. 41 (1980) 151.
[3] D. Lerche, J. Theor. Biol. 104 (1983) 231.
[4] G. Bell, M. Dembo, P. Bongrand, Biophys. J. 45 (1984) 1051.
[5] J.K. Angarska, K.D. Tachev, I.B. Ivanov, P.A. Kralchevsky, E.F. Leonard, in: S. Ohki (Ed.), Cell and Model Membrane Interactions, Plenum, New York, 1991, p. 199.
[6] K. Dolowy, in: A.S.G. Curtis, J.D. Pitts (Eds.), Cell Adhesion and Motility, Cambridge University Press, Cambridge, 1980, p. 39.
[7] D. Gingell, I. Todd, Biophys. J. 26 (1979) 507.
[8] D. Gingell, I. Todd, J. Cell Sci. 41 (1980) 135.
[9] A.S.G. Curtis, J. Cell Biol. 19 (1964) 199.
[10] A. Albersdörfer, T. Feder, E. Sackmann, Biophys. J. 73 (1997) 245.
[11] I.B. Ivanov, A. Hadjiiski, N.D. Denkov, T.D. Gurkov, P.A. Kralchevsky, S. Koyasu, Biophys. J. 75 (1998) 545.
[12] I. Weber, E. Wallraff, R. Albrecht, G. Gerisch, J. Cell Sci. 108 (1995) 1519.
[13] C. Foa, J.-L. Mege, C. Capo, A.-M. Benoliel, J.-R. Galindo, P. Bongrand, in: P. Bongrand (Ed.), Physical Basis of Cell–Cell Adhesion, CRC Press, Boca Raton, FL, 1988, p. 191.
[14] E.F. Leonard, I. Rahmin, J.K. Angarska, C.S. Vassilieff, Ann. N.Y. Acad. Sci. 516 (1987) 502.
[15] G.A. Truskey, J.S. Burmeister, E. Grapa, W.M. Reichert, J. Cell Sci. 103 (1992) 491.
[16] S.K. Robertson, S.G. Bike, Langmuir 14 (1998) 928.
[17] H. Wolf, D. Gingell, J. Cell Sci. 63 (1983) 101.
[18] E. Donath, D. Gingell, J. Cell Sci. 63 (1983) 113.
[19] B.V. Derjaguin, Acta Physicochim. USSR 12 (1940) 181.
[20] H.M. Princen, S.G. Mason, J. Colloid Sci. 20 (1965) 156.
[21] I.B. Ivanov, B.V. Toshev, Colloid Polym. Sci. 253 (1975) 593.
[22] W. Helfrich, R.-M. Servuss, Nuovo Cimento D3 (1984) 137.
[23] E.A. Evans, Adv. Colloid Interface Sci. 39 (1992) 103.
[24] E.A. Evans, R. Skalak, Mechanics and Thermodynamics of Biomembranes, CRC Press, Boca Raton, FL, 1980.
[25] E.A. Evans, J.C. Fung, Microvasc. Res. 4 (1972) 335.
[26] A.J. McConnell, Application of Tensor Analysis, Dover, New York, 1957.
[27] W. Helfrich, Z. Naturforsch. 28c (1973) 693.
[28] H.J. Deuling, W. Helfrich, Biophys. J. 16 (1976) 861.
[29] H.J. Deuling, W. Helfrich, J. Phys. 37 (1976) 1335.
[30] P.R. Zarda, S. Chien, R. Skalak, J. Biomech. 10 (1977) 211.
[31] U. Seifert, K. Berndl, R. Lipowsky, Phys. Rev. A 44 (1991) 1182.
[32] B.L.-S. Mui, H.-G. Dobereiner, T.D. Madden, P.R. Cullis, Biophys. J. 69 (1995) 930.
[33] R. Bruinsma, Proc. NATO Adv. Inst. Phys. Biomater: NATO ASI Ser. 332 (1995) 61.
[34] A.G. Volkov, D.W. Deamer, D.L. Tanelian, V.S. Markin, Liquid Interfaces in Chemistry and Biology, Wiley, New York, 1998.
[35] I.B. Ivanov, P.A. Kralchevsky, in: I.B. Ivanov (Ed.), Thin Liquid Films, Marcel Dekker, New York, 1988, p. 49.
[36] P.A. Kralchevsky, J. Colloid Interface Sci. 137 (1990) 217.
[37] J.C. Eriksson, S. Ljunggen, P.A. Kralchevsky, J. Colloid Interface Sci. 161 (1993) 133.
[38] P.A. Kralchevsky, J.C. Eriksson, S. Ljunggren, Adv. Colloid Interface Sci. 48 (1994) 19.
[39] S. Ljunggren, J.C. Eriksson, P.A. Kralchevsky, J. Colloid Interface Sci. 191 (1997) 424.
[40] H.M. Princen, in: E. Matijevic (Ed.), Surface and Colloid Science, vol. 2, Wiley, New York, 1969, p. 1.
[41] E.A. Evans, R.M. Hochmuth, in: A. Kleinzeller, F. Bronner (Eds.), Current Topics in Membranes and Transport, vol. 10, Academic Press, New York, 1978, p. 1.
[42] E.A. Evans, Biophys. J. 43 (1983) 27.
[43] A.I. Rusanov, V.A. Prokhorov, Interfacial Tensiometry, Elsevier, Amsterdam, 1996.

[44] A.W. Adamson, A.P. Gast, Physical Chemistry of Surfaces, 6th Edition, Wiley-Interscience, New York, 1997.
[45] S. Nir, C.S. Vassilieff, in: I.B. Ivanov (Ed.), Thin Liquid Films, Marcel Dekker, New York, 1988, p. 207.
[46] P. Richmond, J. Chem. Soc. Faraday Trans. II 70 (1974) 1066.
[47] P. Richmond, J. Chem. Soc. Faraday Trans. II 71 (1975) 1154.
[48] J.A. de Feijter, A. Vrij, J. Colloid Interface Sci. 70 (1979) 456.
[49] S. Kawahata, H. Ohshima, N. Muramatsu, T. Kondo, J. Colloid Interface Sci. 138 (1990) 182.
[50] B.V. Derjaguin, Theory of Stability of Colloids and Thin Films, Plenum, Consultants Bureau, New York, 1989.
[51] M.J. Grimson, P. Richmond, C.S. Vassilieff, in: I.B. Ivanov (Ed.), Thin Liquid Films, Marcel Dekker, New York, 1988, p. 275.
[52] T. Arvinte, B. Shulz, A. Cudd, C. Nicolau, Biochim. Biophys. Acta 981 (1989) 51.
[53] Y.H. Tokmakov, Investigation on the red blood cell adhesion behavior, Diploma Work, Department of Biology, University of Shoumen, 1992.
[54] O.E. Panov, Influence of temperature on the adhesion behavior of red blood cells, Diploma Work, Department of Biology, University of Shoumen, 1994.
[55] N. Goldman, Fluorescent Antibody Methods, Academic Press, New York, 1968, pp. 97–124.